Materials Research. 2023; 26(suppl. 1):e20220532
DOI: https://doi.org/10.1590/1980-5373-MR-2022-0532

Maraging 300 Steel Plasma Welding Characterization for Aerospace Application

***Camilla Pessanha Schiavo*[a,b*], *Tiago Alegretti Zucarelli*[b], *Danieli Aparecida Pereira Reis*[a]**

[a]*Universidade Federal de São Paulo (UNIFESP), São José dos Campos, SP, Brasil.*
[b]*Instituto de Aeronáutica e Espaço (IAE), São José dos Campos, SP, Brasil.*

Received: December 09, 2022; Revised: May 31, 2023; Accepted: July 05, 2023

Maraging steel is a special class of high-strength steels that are hardened by the precipitation of intermetallic compounds at temperatures close to 480 °C, without carbon transformation. Since its development, it has been used for strategic applications (nuclear energy, defense, and aerospace areas) and the mastery of its process and application has been constantly improved. This study aimed to characterize the weld regions of a maraging 300 steel used to manufacture a rocket motor case. Welded samples of maraging 300 steel were subjected to metallurgical and mechanical characterization. Microstructural analysis showed three different zones in the hardness range of 291 to 465 HV and reduced toughness. X-ray diffraction showed metallic phases in each region, evidencing the increase of the austenite phase. Based on the results obtained, maraging steel has great potential for aerospace applications, with excellent strength even when subjected to welding.

Keywords: *Maraging, plasma welding, aerospace application, rocket motor case.*

1. Introduction

Maraging steel is an ultra-high strength material manufactured according to the Fe-Ni system (Ni 18-19 wt.%) without carbon addition (maximum 0.003 wt.%). The chemical composition provides the elevated mechanical properties associated with high toughness[1]. Due to the high concentration of Ni, the microstructure of maraging steel at room temperature is martensite; this phase is ductile (BCC) unlike the martensite Fe-C system (BCT), which is hard and fragile. The main strength mechanism of maraging steel is the precipitation of intermetallic compounds during the aging treatment, which act as barriers for dislocation. The combination of a ductile matrix and a high precipitation density leads to the combination of mechanical strength and toughness. The aging treatment occurs around 460 to 500 °C, increasing hardness from 3035 to 4853 HRC[2]. Besides the mechanical characteristics, this material has good rolling/forging, machinability, and weldability, which makes it a strong candidate for strategy application, such as: solution treatment condition for military, aerospace, and nuclear industry[2-5].

The heat treatment of maraging steel basically consists of a solution at temperatures above 800 °C and then a low-temperature aging stage (460–500 °C). The solution stage results in a microstructure characterized by lath martensite, a body-centered cubic (BCC) with a high discordance density[6,7]. Optical microscopy analysis of a sample of maraging 350 in the solution condition pointed the presence of lath martensite. X-ray diffraction (XRD) analysis confirmed the previous result, showing martensite peaks at (110), (200), (211), and (220) plans[6].

Maraging steel may be welded using fusion welding techniques, such as gas tungsten arc welding (GTAW), plasma arc welding (PAW), and laser beam welding (LBW)[8]. Welding is the most important bonding process of the material used today, defined as a local adhesion process to maintain the characteristics on the material over the weld bead. This process may or may not use local melting, but it has significant heat generation and plastic deformation most of the time[9].

1.1. PAW Process

Among fusion welding processes, PAW is a derivative of GTAW, since it uses a tungsten non-consumable electrode, an inert gas (usually argon) to produce the arc and protect the melt metal[10-13]. The PAW process has a constricting nozzle, similar to a funnel, that confines the plasma and results in better distribution, energy concentration, and raises the fusion efficiency. Due to the constricting nozzle, PAW brings benefits, such as heat with temperatures above 25,000 °C, increased displacement speed, better bead penetration, reduced heat affected zone (HAZ), simplified joint preparation procedures, and greater possibility to vary the distance between the material and the torch[11,13-16].

PAW processes can be classified into three types, depending on the current used: micro PAW, melt-in PAW, and keyhole PAW. Micro plasma needs low current (0.1–15 A) during the welding process to join pieces with thicknesses from 0.01 to 1.5 mm[11,13,15,17]. The melt-in technique is usually applied to workpieces up to 2.4 mm thick, using a current of about 15 to 400 A and a manual welding process with low gas flow and one or more passes[10,12,17]. Finally, the keyhole mode is used when the workpiece is up 2.5 mm thick, with a current of more than 400 A[12,15]. This mode forms a hole that crosses the molten pool where the liquid metal penetrates, solidifying at the back of it. During welding, this hole moves according to the displacement of the torch. The molten metal is forced to

*e-mail: cschiavo2001@yahoo.com.br

move around the plasma jet forming the weld puddle behind the hole, closing it and forming the weld bead[11-14].

1.2. Weld bead microstructure

Regardless of the chosen process, the weld bead will show changes in material proprieties particularly related to plastic deformation or caused by temperature variation. Especially in the fusion welding process, the heat sources used are so powerful that the material presents different metallurgical characteristics. The weld bead macrostructure has three different zones: melted zone (MZ), heat affected zone (HAZ), and base material (BM)[1617]. In the MZ, the material reaches its melting temperature and the austenite formed turns into martensite during cooling. In maraging steel, this region consists of Fe-Ni martensite with 30 HRC hardness. In the HAZ, the microstructure of the material changes due to temperature, which reaches levels up to the critical temperature. This zone commonly has martensite and a retained fine-grain austenite. The BM presents few microstructural changes because it is farthest from the weld bead[18-21].

Today, in Brazil, especially in the aerospace industry, ultra-high strength steels, such as AISI 4340 and AISI 300M, have been replaced by maraging steel. The suborbital rocket motor case design is an example of this type of application. The Institute of Aeronautics and Space (IAE) has been developing a suborbital rocket consisting of a two-stage solid propellant vehicle, equipped with payload, recovery, and service systems[22]. The constant development of this vehicle contributes to the payload design, payload recovery system, and the evolution of tracking and data acquisition systems[23]. The rocket motor case is cylindrical and was constructed from calendered sheets with circumferential and longitudinal welding[24] (Figure 1).

This study evaluates the performance, considering mechanical and microstructural characteristics, of PAW-welded maraging 300 steel used in the manufacture of suborbital rocket motor cases.

2. Experimental Details

2.1. Material specifications and chemical analysis

For this study, it was used maraging 300 sheets, produced by vacuum arc remelting (VAR) and heat treated after steel solidification (820 °C during 1 hour). Two pieces of this rolled maraging 300 sheet were welded according to the AMS 6521C specification[25] measuring 3.3 mm × 100 mm × 300 mm (thickness × width × length). The welding wire used was MAR 300, Ø 9 mm, in line with the AMS 6463D specification[26]. Both materials were chemical analyzed to certify that they were in accordance with specifications. Chips were analyzed by direct combustion using LECO CS-200 to obtain composition C and S, according to the ASTM E30 specification[27]. Ni and Si were determined by gravimetry, in accordance with the ASTM E30 specification[27]. Other elements (Mn, Mo, Co, Ti, and Al) were determined using atomic absorption in SPECTRAA20 PLUS. The samples was prepared using 1 g of the material and nitro-muriatic acid (30 ml HCl + 10 ml HNO_3 + ionized water) on a plate electrically heated to 200–250 °C.

2.2. Welding parameters

The samples were welded by PAW, using one weld pass without defects and the following parameters: welding speed (200 mm/min), welding wire speed (0.6 m/min), welding current (120 A) and welding wire (MAR300). Figure 2 shows a schematic view of the welding groove.

2.3. Microstructural analyses

The samples were prepared according to the ASTM E3 standard[28]. Vilella's etchant (5 ml HCl, 2 g picric acid, and 100 ml ethyl alcohol) and the 15-minute immersion technique were used. The sample was analyzed by optical microscopy, using ZEISS Axio Imager 2, over its three different zones melting zone (MZ), heat affect area (HAZ) and base material (BM). The different sample phases were identified using Rigaku Ultima VI XRD, CuKα radiation source (λ = 1.5406 A), 40 kV voltage, 30 mA current, 30° to 90° angular range, 0.02°/5 s angular pass, and 2 mm slit.

2.4. Analysis of mechanical proprieties

Tension was evaluated in accordance with the ASTM E8/E8M[29] subsize parameters. Tests used three samples with reinforced/root weld beads. A universal machine model MTS 810 23M, with 250 kN capacity and hydraulic grabs to prevent any sample from slipping, and the FlexTest 40 computer control system were used for data analysis. Hardness was analyzed using EMCO-TEST, DuraScan G5, and the EMCO Works analysis system. Moreover, a square diamond indenter (0.3 kg load per 15 s and 65 indentations) was used.

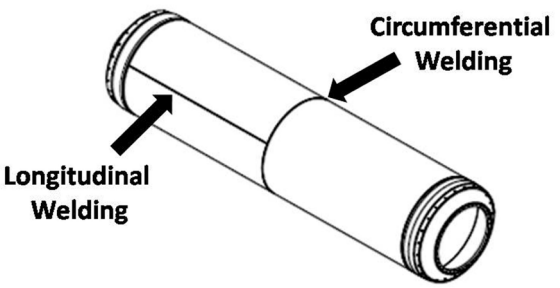

Figure 1. Schematic representation of a rocket motor case with longitudinal and circumferential weld.

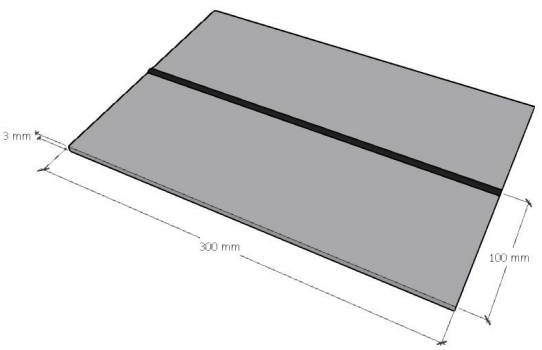

Figure 2. Schematic view of the weld.

3. Results

3.1. Chemical composition analysis

Table 1 presents the chemical composition of both the maraging steel sheets and the welding wire used and the values established by the AMS 6521C[25] and AMS 6463D[26] standards for each element. The chemical compositions analyzed were in line with these standards.

3.2. Optical microscopy (OM)

The weld bead microstructure had homogenous weld, emptiness, porosity, and free blow holes (Figure 3). Figure 4 shows the microstructural evolution and the three zones in (a), the MZ in (b), the HAZ in (c), and the BM in (d). The MZ had a dendrite structure characteristic of a welded region, with a high concentration of reversed austenite. In both the HAZ and the BM, the martensite microstructure was the same, but the HAZ had coarse grains and higher density of reversed austenite due to thermal input. Finally, the BM had a martensite structure typical of the heat treatment condition of the maraging 300 solution, without significant changes.

The microstructural results are in accordance with the literature regarding the presence of centrally oriented welding dendrites in the MZ, followed by the two different areas with a large grain size (HAZ1 and HAZ2) and the metal base region without any microstructural transformation[13,20].

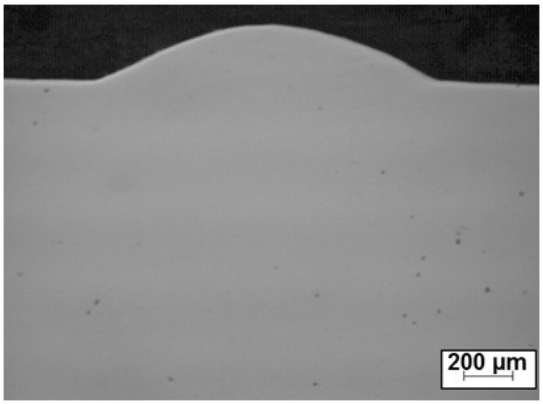

Figure 3. Macro view of the weld.

3.3. X-Ray diffraction (XRD)

Figure 5 shows the different welding areas where XRD was applied, highlighting the martensite peaks with the symbol ◆ (110), (200) and (211) and the austenite peaks with the symbol Δ - (111) and (200). Both phases achieved (martensite and austenite) were in accordance with the literature[30-33]. Some studies observed a higher martensite peak around 45° and other martensitic phase diffraction peaks around 65° and 85°[30,3233]. The diffractogram generated in XDR, supported by the HighScore Plus software, made it possible to quantify the perceptual phase using the Rietveld method. The MZ consisted of 88% martensite and 12% austenite and the BM, 83% martensite and 17% austenite.

3.4. Tensile test

Figure 6 presents the tensile stress-strain curves for three welded samples (WS_1, WS_2, and WS_3) and the reference value of the sample as received. Table 2 shows the typical

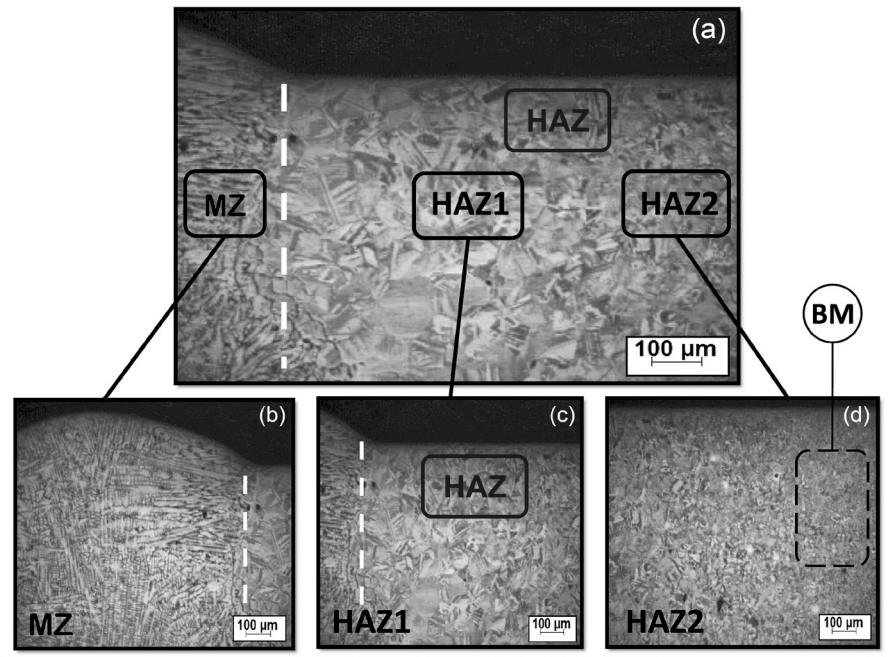

Figure 4. Sample microstructure of different regions: (a) Overview, (b) MZ (Melted Zone); (c) HAZ1 (Heat Affect Zone 1 with coarsed grain size) and HAZ2 (Heat Affect Zone 2 with more refined grain than HAZ1) and (d) BM (Base Material).

Table 1. Maraging 300 steel plate and weld wire MAR 300 wt.%.

		C	Mn	Si	S	Ni	Mo	Co	Al	Ti
Maraging 300 steel plate										
AMS 6521C	lower	-	-	-	-	18	4.6	8.5	0.05	0.5
	upper	0.03	0.1	0.10	0.010	19	5.2	9.5	0.15	0.8
Measured		<0.004	<0.01	0.03	<0.0016	18.6	4.6	8.5	0.09	0.6
Weld wire MAR 300										
AMS 6463D	lower	-	-	-	-	18	4.5	8.0	0.05	0.6
	upper	0.01	0.1	0.1	0.01	19	6.5	9.0	0.15	0.8
Measured		0.007	0.015	0.07	<0.0016	18.3	4.4	9.3	0.12	0.6

Table 2. Tensile values of maraging 300 for the base metal and PAW-welded samples.

Condition	Sample	σ_y (MPA)	σ_T (MPA)	σ_B (Mpa)
As received	reference	1,080.45	1,167.57	983.01
After Welding samples	WS_1	898.46	1,015.93	509.38
	WS_2	874.17	1,008.61	495.89
	WS_3	941.01	1,068.80	538.68
	Average	**(904.55 ± 33.83)**	**(1,031.11 ± 32.84)**	**(514.65 ± 21.88)**
Literature				
Oliveira[33]		917	1,024	
Silva[34]		975	1,042	

σ_y: Yield Strength; σ_T: Ultimate Tensile Strength; σ_B: Breaking strength; WS_1: Sample 1 Solution Annealed at 820°C; WS_2: Sample 2 Solution Annealed at 820°C; WS_3: Sample 3 Solution Annealed at 820°C.

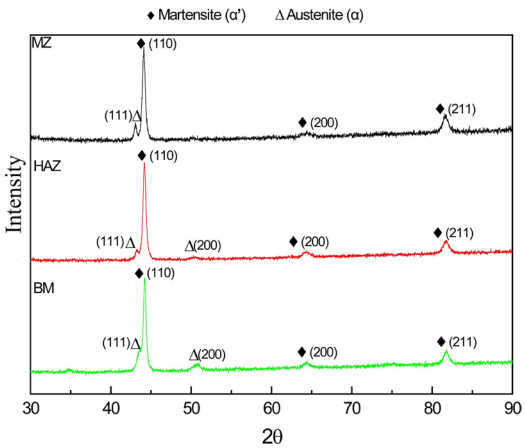

Figure 5. X-ray diffractogram of different sample regions.

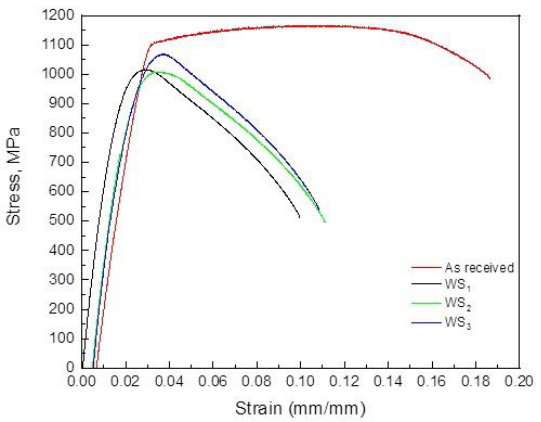

Figure 6. Tensile test graph.

effect of welding on ultimate tensile strength (UTS) and yield strength (YS). Average UTS reduced by around 11% (1031 MPa against 1163 MPa) and average YS reduced by 15% (1071 MPa against 904 MPa). The main effect of welding is the reduction of toughness due to the decrease in tensile strength (σ_t), as shown by the difference in area under curves when comparing the BM with WS_1, WS_2 or WS_3.

The tensile results are in line with Oliveira[33] and Silva[34], who welded maraging 300 steel using PAW (Table 2). They found 917 MPa and 975 MPa for average YS and 1024 MPa and 1042 MPa for average UTS, respectively.

3.5. Hardness survey

Figure 7 shows the hardness analysis. The maximum hardness value was 465 HV, found in HAZ2 (the red region on the map), and the minimum value was 291 HV, found in the MZ (the blue region on the map). The hardness values in the MZ and HAZ1 were similar, varying from 291 HV to 310 HV (around 7%). The figure also shows an increase in hardness in HAZ2, reaching 465 HV in a zone characterized by early precipitation. In HAZ1, the average hardness value was 310 HV(around 31 HRC), which is similar to the average found in the literature[34] (34 HRC; around 336 HV).

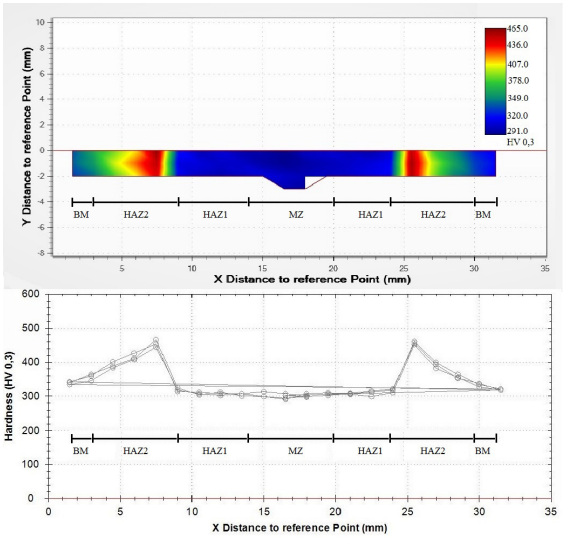

Figure 7. Hardness analysis.

4. Discussion

The chemical composition of maraging steel gives this material special characteristics. The concentration of the metallic phase was similar in the MZ (88% martensite and 12% austenite) and the BM (82% martensite and 18% austenite). The reason for this phenomenon was the nickel concentration, which causes the material to obtain the martensite structure under different cooling rates. Hardness in the MZ was close to that in the BM, as its levels in maraging steel in solution heat treatment condition increase from the martensite structure. After the aging treatment, the hardness value is different because the kinematic precipitation is not the same in the MZ (dendrite) and the BM (lath martensite).

5. Conclusions

This study showed the concentration of the metallic phase and evaluated the hardness, microstructure, and strength of PAW-welded maraging steel.

- The PAW process created four different zones in the sample due to the decreasing temperature gradient and the propagation of heat conduction: base material (BM), heat affect zone 1(HAZ1), heat affect zone 2 (HAZ2), and melted zone (MZ). In HAZ1, hardness increased, and HAZ2 had a higher hardness value due to more intermetallic precipitation.
- Maraging steel had a similar concentration of the metallic phase (martensite and austenite) in the MZ and the BM, showing similarity between the weld bead and the base material.
- In the MZ, hardness was closer to the values in the BM. In HAZ1 and HAZ2, hardness increased due to the precipitation of intermetallic compounds (around 37% when compared with the BM). In order to obtain a more homogeneous hardness after welding, we recommend heat treating the solution after the welding process.
- The weld bead had high UTS and yield strength. The main effect of the welding was reduced toughness due to the decrease in breaking strength.

6. Acknowledgements

The authors thank FINEP, FAPESP, CAPES and CNPq for their financial support.

7. References

1. Kapoor R, Kumar L, Batra IS. A dilatometric study of the continous heating transformations in 18wt.% Ni Maraging steel of grade 350. Mater Sci Eng. 2003;352(1-2):318-24.
2. Rohrbach K, Schmidt M. Maraging steels. In: ASM International. ASM handbook, volume 1: properties and selection: irons, steels, and high-performance alloys. 10th ed. Materials Park: ASM International; 1990. p. 1869-87.
3. Giacomelli JP, Freitas FE, Reis AG, Oliveira AC, Santos VR, Reis DAP. Avaliação dos parâmetros de nitretação por laser de CO_2 no aço Maraging 18Ni (300) para melhoria da resistência à oxidação. Tecnol Metal Mater Min. 2021;18:e2363.
4. Reis AG, Reis DAP, Abdalla AJ, Couto AA, Otubo J. An in situ high-temperature X-ray diffraction study of phase transformations in Maraging 300 steel. Defect Diffus Forum. 2017;371:73-7.
5. Reis AG, Reis DAP, Abdalla AJ, Couto AA, Otubo J. Short-term creep properties and fracture surface of 18 Ni (300) Maraging steel plasma nitrided. Mater Res. 2017;20:2-9.
6. Carvalho LG, Andrade MS, Padilha AF. Análise da cinética da transformação martensítica em um aço Maraging da série 350. In: 68º Congresso Anual da ABM; 2013 Jul/Aug 30-3; Belo Horizonte. Proceedings. São Paulo: Associação Brasileira de Metalurgia, Materiais e Mineração; 2013. p. 981-90.
7. Santana SIV, Brandão LP. Estudo de parâmetros que controlam a nucleação da austenita revertida nos aços Maraging 350. Rev Mil Ciênc Tecnol. 2019;36:52-5.
8. Sakai PR, Lima MSF, Fanton L, Gomes CV, Lombardo S, Silva DF et al. Comparison of mechanical and microstructrural characteristics in Maraging 300 steel welded by three different processes: laser, plasma and TIG. Procedia Eng. 2015;114:291-7.
9. Ferreira IO, Morais VLA, Sampaio GG, Morais WA. Desempenho de soldadores em qualificação: aspectos humanos e diferenças entre chapas e tubos. In: XIII Simpósio Internacional de Ciências Integradas; 2016 Oct 24-26; Guarujá. Proceedings. Ribeirão Preto: UNAERP; 2016. p. 1-8.
10. Modenesi PJ, Marques PV. Soldagem 1: introdução aos processos de soldagem. Belo Horizonte: Universidade Federal de Minas Gerais; 2000.
11. Díaz VMV. Influência dos parâmetros e variáveis de soldagem a plasma sobre as características da solda com ênfase na análise da abertura e no fechamento do keyhole [dissertation]. Florianópolis: Universidade Federal de Santa Catarina; 1999.
12. Liu ZM, Cui SL, Luo Z, Zhang CZ, Wang ZM, Zhang YC. Plasma arc welding: process variants and its recent developments of sensing, controlling and modeling. J Manuf Process. 2016;23:315-27.
13. Marqueti PR. Estudo de juntas de aço Maraging 300 soldadas por plasma e tratadas termicamente após a soldagem [dissertation]. São José dos Campos: Universidade Federal de São Paulo; 2017.
14. Modenesi PJ, Marques PV, Bracarense AQ. Soldagem: fundamentos e tecnologia. 3rd ed. Belo Horizonte: Editora UFMG; 2011. 363 p.
15. Sahoo A, Tripathy S. Development in plasma arc welding process: a review. Mater Today Proc. 2021;41:363-8.

16. Selvan MCP, Rammohan N, Salins SS. Plasma Arc Welding (PAW) - a literature review. Am Int J Res Sci Technol Eng Math. 2015;15(595):181-6.
17. Harris ID. Plasma arc welding. In: ASM International. ASM handbook, volume 6: welding, brasing and soldering. Materials Park: ASM International; 2004. p. 605-15.
18. Cary HB. Modern welding technology. Englewood Cliffs: Prentice-Hall; 1979.
19. Baskutis S, Žunda A, Kreivaitis R. Mechanical properties and microstructure of aluminium alloy AW6082-T6 joints welded by double-sided MIG process before and after aging. Mechanika. 2019;25(2):107-13.
20. Lang FH, Kenyon N. Welding of maraging steels [Internet]. New York: Welding Research Council; 1971 [cited 2021 Jan 19]. 41 p. WRC bulletin 159. Available from: https://nickelinstitute.org/media/8d919459e02fda3/ni_inco_584_weldingofmaragingsteels.pdf
21. Gomes CV, Barboza MJR, Silva DF, Lombardo S, Abdalla AJ. Caracterização microestrutural e mecânica do aço Maraging 300 soldado por processo a laser e a plasma e posteriormente envelhecido. Rev Bras Apl Vac. 2016;35(1):25-30.
22. Garcia A, Yamanaka SSC, Barbosa AN, Bizarria FCP, Jung W, Scheuerpflug F. VSB-30 sounding rocket: history of flight performance. J Aerosp Technol Manag. 2011;3(3):325-30.
23. Silva FM, Perondi LF. A proposal of a life-cycle for the development of sounding rockets missions. J Aerosp Technol Manag. 2021;13:1-18.
24. Palmerio AF. Introdução à tecnologia de foguetes. São José dos Campos: SindCT; 2016. 302 p.
25. Society of Automotive Engineers. SAE AMS 6521C-1991: steel sheet, strip, and plate, Maraging 18.5Ni 9.0Co 4.9Mo 0.65Ti 0.10Al, consumable electrode melted, solution heat treated. USA: American National Standards Institute; 1991.
26. Society of Automotive Engineers. SAE AMS 6463D-2009: wire, steel welding 18.5 Ni 8.5 Co 5.2 Mo 0.72 Ti 0.10 Al (Maraging 300), vacuum melted, environment controlled packing. USA: American National Standards Institute; 2013.
27. ASTM International. ASTM E30-89: tests methods for chemical analysis of steel, cast iron, open-hearth iron, and wrought iron. West Conshohocken: ASTM International; 1989.
28. ASTM International. ASTM E3-11: standard guide for preparation of metallography specimens. West Conshohocken: ASTM International; 2011.
29. ASTM International. ASTM E8/E8M: standard test methods for tension testing of metallic materials. West Conshohocken: ASTM International; 2021.
30. Marchetto LRO, Briguente LANS, Reis DAP, Lopez JO, Reis AG. Microstructural evaluation of Maraging 300 steel surface treated by Nd:YAG laser. Braz J Dev. 2022;8(3):15918-24.
31. Florez MAC, Sousa ABF, Mata SAS, Bastos M No, Silva MJG. Síntese e caracterização de um filme de óxido tipo espinélio obtido durante o tratamento de envelhecimento do aço Maraging 300 em atmosfera de N_2/vapor. In: 74º Congresso Anual da ABM Internacional; 2019 Oct 1-3; São Paulo. Proceedings. São Paulo: Associação Brasileira de Metalurgia, Materiais e Mineração; 2019. p. 1-12.
32. Reis AG. Comportamento mecânico do aço Maraging 300 solubilizado, envelhecido e nitretado por plasma [thesis]. São José dos Campos: Instituto Tecnológico de Aeronáutica; 2015.
33. Oliveira RC. Caracterização mecânica e microestrutural dos aços 300 M e Maraging 300 após soldagem a plasma [dissertation]. São José dos Campos: Instituto Tecnológico de Aeronáutica; 2015.
34. Silva DF. Caracterização mecânica e microestrutural do aço Maraging 300, soldado a plasma e submetidas a reparos [dissertation]. Guaratinguetá: Universidade Estadual Paulista "Júlio de Mesquita Filho", Faculdade de Engenharia; 2014.